Mechanism of B removal by solvent refining of silicon in Al–Si melt with Ti addition

Boyuan Ban [a], Jingwei Li [a], Xiaolong Bai [a], Qiuxiang He [a], Jian Chen [a, *], Songyuan Dai [a, b]

[a] Key Laboratory of Novel Thin Film Solar Cells, Institute of Applied Technology, Hefei Institutes of Physical Science, Chinese Academy of Sciences, Hefei, 230031, China
[b] State Key Laboratory of Alternate Electrical Power System with Renewable Energy Sources, North China Electric Power University, Beijing, 102206, China

A B S T R A C T

Solvent refining of Al–Si–B alloy samples with different amounts of Ti additions are carried out, which confirms a high B removal rate with excessive Ti addition. An apparent segregation coefficient is introduced to characterize the segregation between primary Si and Al–Si melt, which are determined to be 0.0471 with 575 ppma Ti addition at the cooling rate of 50 mK·s^{-1}. Temperature dependence of $X_{\text{Ti(l) in Al–Si melt}} X^2_{\text{B(l) in Al–Si melt}}$, individual Ti and B contents in the Al-29.3at.%Si melt from 1323 to 1123 K are calculated. It proves that TiB$_2$ precipitates before the primary Si formation, which causes the decrease of B contents in the Al–Si melt and contributes to the high B removal rate. Moreover, BSE/SEM observation of TiB$_2$ and (Al,Ti,Si) phase indicates a new competitive reaction mechanism in Al–Si–Ti–B system.

© 2016 Elsevier B.V. All rights reserved.

1. Introduction

In light of increased awareness of environment protection and need for renewable green energy sources, much attention is given to the use of solar cells, especially the most widely-used crystalline silicon solar cells. The material resource for crystalline Si solar cells is solar grade Si (SoG-Si). Currently, the production process of SoG-Si [1], via the traditional Siemens process or its modified alternatives, is fairly energy intensive and environment-unfriendly [2,3]. In order to reduce its energy consumption and environment pollution, metallurgical refining processes of SoG-Si using metallurgical grade Si (MG-Si) as a starting material have been developed. These include slag treatment [4], plasma treatment [5], and solvent refining [6].

Boron (B) is one of the major impurities in Si and should be reduced to lower than 1 ppma for solar cell application. Because the segregation coefficient of B in solid/liquid Si, 0.8 [7], is much larger than those of most metallic impurities in Si, thus the ordinary directional solidification refining is not effective for B removal. In recent years, plasma refining processes such as H$_2$O-added Ar plasma treatment have been developed [8], using the heat of the

plasma torch to activate H$_2$O and producing volatile H–B–O species that are evaporated to remove B. However, the high cost of the equipment and the large energy consumption limit this technique from industrial application.

Solvent refining with Al–Si alloy is a very promising process to produce SoG-Si at large scale with low cost [6,9–11] and one of the few metallurgical Si purification processes that are realized in industrial scale [12]. The purification can be achieved by redistributing the impurities in the solid/liquid interface. Compared with directional solidification of Si(1700–1800 K), solvent refining with Al–Si alloy (850–1500 K) is carried out at much lower temperature, and the removal of B is more efficient [9]. Yoshikawa et al. [13] reported B removal by solidification refining of Si in the Si–Al melt with excessive Ti addition, and the solubility of TiB$_2$ in the Al–Si melt by thermodynamic calculation. Johnston et al. [14] reported that adding Ti to molten Si is not effective for removing B or P, serving only to contaminate the Si with Ti.

Our recent research proved that kinetics is also an important factor controlling the B removal efficiency [11]. In this work, different amounts of Ti are added into Al-29.3at%Si alloy. The effect of different Ti additions on the macrostructures of Al–Si ingots, B and P removal, and precipitation of TiB$_2$ particles in the Al–Si melt are studied. The activity coefficient of Ti–2B atoms groups in molten Al and Si in liquid standard state at infinite dilution, temperature dependence of $X_{\text{Ti(l) in Al–Si melt}} X^2_{\text{B(l) in Al–Si melt}}$ and the

individual Ti and B contents in the Al-29.3at.%Si melt from 1323 to 1123 K are calculated. The BSE/SEM image of TiB$_2$ particles and (Al,Ti,Si) phase are studied. The results in this research reveal the mechanisms of B removal by solvent refining with Ti addition. Due to the very high boron removal rate achieved in this work, it might suggest a new method to significantly improve the refining process of the SoG-Si and widely broaden the source Si materials that can be used in industrial Al–Si solvent refining process, which might revolutionize the SoG-Si production industry.

2. Materials and methods

To study the effect of Ti addition thoroughly and avoid the effect of other elements that may be brought in by MG-Si and commercial Al, the Al–Si alloys were prepared by mixing of SoG-Si (6N), high purity Al (99.96%), Si–B master alloy, Si–P master alloy and Si–Ti master alloy. A total of 80 g raw materials (56 g Al and 24 g Si) were put in an alumina crucible (O.D. = 35 mm, Depth = 70 mm). Parallel experiments with four different amounts of Ti additions were carried out in this work. The parameters of each experiment are summarized in Table 1.

The experimental process was described in our previous publication [15]. The crucibles were placed in an electric resistance furnace, heated to 1323 K in Ar atmosphere, then held for 3 h. After melting, the samples were cooled down quickly to 10 K above the liquidus temperature (1133 K) and then cooled to 833 K, which is 17 K below the eutectic temperature with a pre-determined cooling rate (50 mK·s^{-1}). Then the solidified sample was taken out from the furnace and leached in diluted HCl and HNO$_3$. After the acid leaching, the Si flakes were rinsed with deionized water, dried and separated.

The separated primary Si flakes of each sample, which were considered as refined Si, were measured by sieve analysis. The macrostructure of the Al–Si alloy ingots were obtained using an image scanner. Microstructure of the Si samples and composition of intermetallic compounds in the samples after the solvent refining processes were examined by scanning electron microscope-back scattered electron detector-energy dispersive spectroscopy (SEM-BSE-EDS). In addition, the concentrations of impurities from the refined Si flake samples were analyzed by inductively coupled plasma optical emission spectrometry (ICP-OES).

3. Results and discussion

3.1. Macrostructure of Al–Si ingots

Fig. 1(a) represents the vertical cross section of a sample examined by a digital scanner. Because the experiment is not carried out under vacuum, the sample contains some gas bubbles in the corner. The primary Si flakes display needle-like morphology and stretch out until meet another primary Si flake. Although with different amounts of Ti additions, the macrostructures of different samples remain the same.

To evaluate the size distribution and average mass of the

Table 1
List of experiments.

Experiment number	Initial content (ppma)			Cooling rate (mK·s^{-1})
	B	P	Ti	
E-1	297	88	0	50 mK·s^{-1}
E-2	296	91	63	
E-3	304	87	172	
E-4	295	88	575	

primary Si flakes, a sieve analysis is carried out and fineness number (FN) of each sample is examined. The FN defined by American Foundry Society, presents the average particle size along with its distribution and larger FN means finer flake size distribution. This is explained by the following Eq. (1):

$$FN = \frac{\sum_1^n (S_i \times W_i)}{\sum_1^n W_i} \tag{1}$$

where S_i is the fineness modulu of each sieve, W_i is the weight of the remaining flakes in the sieve, and n is the number of sieves. Fig. 1(b) shows the FN of each sample. From sample E-1 to E-4, the FNs remain the same. These results show that the Ti addition has no significant influence on the growth of the primary Si flakes.

3.2. Impurities removal in the primary Si

Fig. 2 shows the impurities contents in the primary Si examined by ICP-OES. Four important impurities (B, P, Al, Ti) show three different trends with increasing amount of Ti addition. With the increasing Ti addition, the B contents in the primary Si fall from 232 ppma in sample E-1, to 167 ppma in sample E-2, 85 ppma in sample E-3, and 12 ppma in sample E-4, and the P contents in the primary Si fluctuate slightly around 32 ppma. The Al contents in the primary Si increase from 509 ppma (E-1) to 835 ppma (E-4), while the Ti contents in the primary Si increase rapidly from 0.2 ppma (E-1) to 116 ppma (E-4). The Ti additions contribute remarkably to the B removal but have no significant effect on P removal, while the Al contents in the primary Si increase with increasing Ti contents in the primary Si, indicating a strong affinity between Ti–B and Al–Ti during the solidification.

An apparent segregation coefficient, k_{app} is introduced to characterize the B removal during the solidification, an equation similar to Scheil equation is derived for the calculation of the solid composition as a function of f_S:

$$X_B = k_{app}X_{B\ ini}(1 - f_s)^{k_{app}-1} \tag{2}$$

where X_B is the B content (mole percentage) in the primary Si, $X_{B\ ini}$ is the initial B content (mole percentage) in the Al–Si melt, and f_S is the fraction of the primary Si.

Considering that the total amount of solute in the solid must be conserved, the formula is obtained by integration of Eq. (2):

$$\int_0^{f_S} k_{app}X_B(1 - s)^{k_{app}-1}ds = \overline{X_B}f_S \tag{3}$$

$$k_{app} = \log_{1-f_s}\left(1 - \frac{\overline{X_B}f_S}{X_{B\ ini}}\right) \tag{4}$$

where $\overline{X_B}$ is the average composition (mole percentage) of B in the primary Si obtained by ICP-OES. In this work, for the Al -29.23 at.% Si, f_S is 0.193. From Eq. (4), k_{app} are obtained as 0.763, 0.541, 0.261 and 0.0471 for sample E-1, E-2, E-3 and E-4, respectively.

Because the solidification is a non-isothermal process, so k_{app} is actually an average of segregation coefficient of the solidification temperature ($\overline{k_B}$) range. $\overline{k_B}$ can be written as Eq. (5):

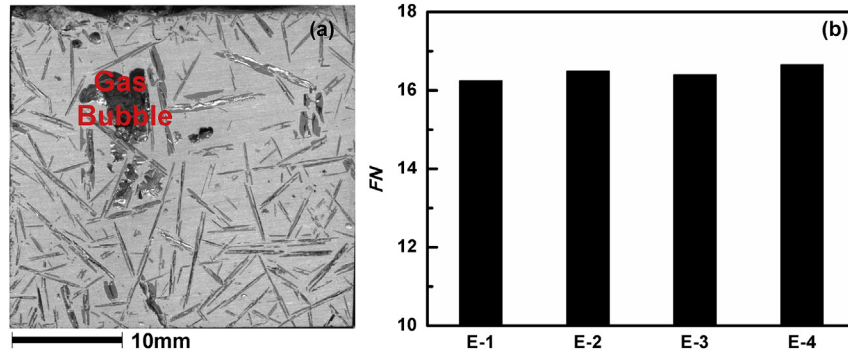$$\overline{k_B} = \frac{1}{T_L - T_E}\int_{T_E}^{T_L} k_B(T)dT \tag{5}$$

Fig. 1. (a) Vertical cross section of a sample, (b) Size (*FN*) of the primary Si flakes in each sample.
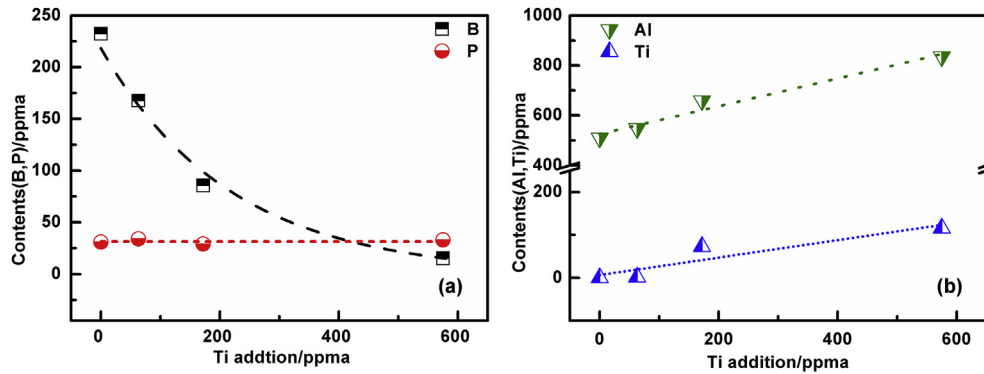

Fig. 2. Impurities contents in the primary Si flakes: (a) B, P contents, (b) Al, Ti contents.

where T_L is the liquidus temperature of the Al-29.3at.%Si melt (1123 K), T_E is the eutectic temperature of the Al−Si melt (850 K) and $k_B(T)$ is the segregation coefficient of B which depends on temperature. Yoshikawa et al. [9] calculated the segregation coefficient in Eq. (6) from isothermal experiment data by a least-square method.

$$\ln k_B(T) = 4.23 - \frac{7300}{T} \tag{6}$$

Bring Eq. (6) into Eq. (5), which leads to the following:

$$\overline{k_B} = \frac{1}{1123 - 850} \int_{850}^{1123} Exp\left[4.23 - \frac{7300}{T}\right] dT = 0.0482$$

Compared with the k_{app} calculated by the experiment data, in sample E-4 $k_{app}(E-4) \approx \overline{k_B}$. Whereas in sample E-1, E-2 and E-3, $k_{app}(E-1) > k_{app}(E-2) > k_{app}(E-3) > k_{app}(E-4) \approx \overline{k_B}$, which is shown in Fig. 3. For the solidification in this work is a non-equilibrium process with a relatively high cooling rate, the difference between the k_{app} in non-equilibrium and $\overline{k_B}$ in equilibrium state is inevitable. Without Ti addition, the B atoms are barely removed from the growing primary Si phase. This result contains a huge gap with Yoshikawa's thermodynamic calculation. Because this work is carried out at a relatively low temperature and in a non-equilibrium state, the formation and trapping of boride rather than the diffusion and segregation of the B atoms near the S/L interface might be the main controlling factor of the B removal in the Al−Si melt. With increasing Ti addition, the k_{app} decreases, indicating that Ti atoms can act as a B getter and reduce the B content in the Al−Si melt during the solidification. The formation of TiB_2 will be discussed in the next section.
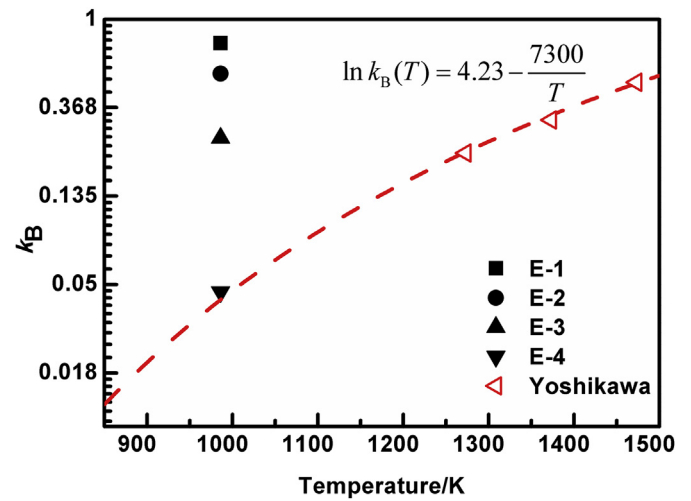

Fig. 3. k_{app} vs. $k_B(T)$.

3.3. Formation of TiB₂ and solubility of Ti and B in the Al−Si melt

Fig. 4 shows standard Gibbs free energies of formation for TiB_2, AlB_2 and SiB_3 calculated by the software of FactSage. It can be found that $\Delta G^{\ominus}_{TiB_2} < \Delta G^{\ominus}_{AlB_2} < \Delta G^{\ominus}_{SiB_3}$, indicating that the TiB_2 particles will precipitate before AlB_2 and SiB_3 in this system. And the reason for $k_{app}(E-1) \gg \overline{k_B}$ discussed in section 3.2 might be the formation and trapping of the AlB_2 particles, resulting in the less effective B removal in the Al−Si system at a relative low temperature. In Fig. 5, the standard Gibbs free energy for TiB_2 formation, $\Delta G^{\ominus}_{TiB_2}$ is defined
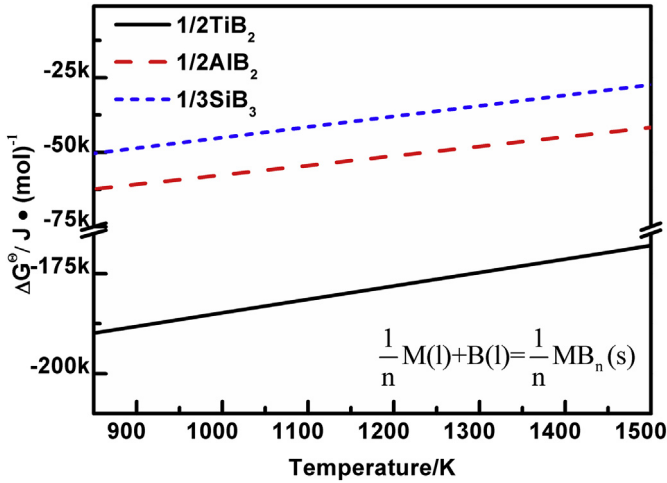
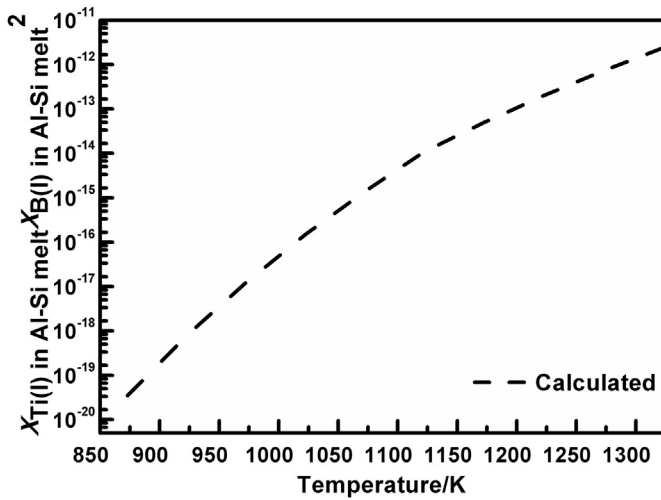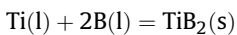Fig. 4. The standard Gibbs free energies of formation for TiB$_2$, AlB$_2$ and SiB$_3$.

Fig. 5. Temperature dependence of $X_{\text{Ti(l) in Al–Si melt}}X^2_{\text{B(l) in Al–Si melt}}$.

in terms of 1:2 liquid Ti and liquid B in standard states. $\Delta G^{\Theta}_{\text{TiB}_2}$ is obtained in the temperature range of 850–1500 K, which leads to the following Eq. (7):

$$\text{Ti(l)} + 2\text{B(l)} = \text{TiB}_2(\text{s})$$

$$\Delta G^{\Theta}_{\text{TiB}_2} = -393392 + 68.21T \left(\text{J·mol}^{-1}\right) \tag{7}$$

In this Al–Si–Ti–B system, Ti and B are not in their standard states and $X_{\text{Ti}} : X_{\text{B}} \neq 1 : 2$, the Gibbs energy change can be expressed as Eq. (8):

$$\Delta G_{\text{TiB}_2} = \Delta G^{\Theta}_{\text{TiB}_2} + RT\ln\frac{a_{\text{TiB}_2}}{a_{\text{Ti(l) in Al–Si melt}}a^2_{\text{B(l) in Al–Si melt}}} \tag{8}$$

where ΔG_{TiB_2} is the Gibbs energy change for TiB$_2$, $\Delta G^{\Theta}_{\text{TiB}_2}$ is the standard Gibbs free energy for TiB$_2$ formation, a_{TiB_2}, $a_{\text{Ti(l) in Al–Si melt}}$ and $a_{\text{B(l) in Al–Si melt}}$ are the activities of TiB$_2$, Ti(l) and B(l) in the Al–Si melt, respectively.

As Ti(l) and B(l) in the Al–Si melt reaches its solubility limits and form TiB$_2$(s) ($\Delta G^f_{\text{TiB}_2} = 0$), TiB$_2$ is in its standard state ($a_{\text{TiB}_2} = 1$), then:

$$\Delta G^{\Theta}_{\text{TiB}_2} = RT \ln X_{\text{Ti(l) in Al–Si melt}}X^2_{\text{B(l) in Al–Si melt}}$$
$$+ RT \ln \gamma_{\text{Ti(l) in Al–Si melt}}\gamma^2_{\text{B(l) in Al–Si melt}} \tag{9}$$

here X_i, and γ_i are mole fraction and activity coefficient of component i, respectively, then $X_{\text{Ti(l) in Al–Si melt}}X^2_{\text{B(l) in Al–Si melt}}$ represents the solubility of Ti–2B atoms groups, and $\gamma_{\text{Ti(l) in Al–Si melt}}\gamma^2_{\text{B(l) in Al–Si melt}}$ represents the activity coefficient of Ti–2B atoms groups.

By applying the Gibbs-Duhem integration method developed by Toop [16], which is expressed by Eq. (10).

$$RT \ln \gamma_{2(1-2-3)} = \left[\frac{x_1}{1-x_2}RT \ln \gamma_{2(1-2)} + \frac{x_3}{1-x_2}RT \ln \gamma_{2(2-3)}\right]_{x_2}$$
$$- (1-x_2)^2\Delta_{\text{mix}}G^E_{1-3\ x_1/x_3} \tag{10}$$

In this system, x_2 is the mole fraction of Ti or B, x_1 is the mole fraction of Al and x_3 is the mole fraction of Si, $\Delta_{\text{mix}}G^E_{1-3\ x_1/x_3}$ denotes the excess Gibbs energy for mixing in the Al–Si melt.

For this Al–Si–Ti–B melt, the relationship for the activity coefficient of Ti–2B can be obtained by Eq. (11) at infinite dilution of Ti–2B atoms groups in the Si–Al melt.

$$RT \ln \gamma_{\text{Ti(l) in Al–Si melt}}\gamma^2_{\text{B(l) in Al–Si melt}}$$
$$= X_{\text{Al in Al–Si melt}}RT \ln \gamma_{\text{Ti(l) in molten Al}}\gamma^2_{\text{Ti(l) in molten Al}}$$
$$+ X_{\text{Si in Al–Si melt}}RT \ln \gamma_{\text{Ti(l) in molten Si}}\gamma^2_{\text{B(l) in molten Si}}$$
$$- 3\Delta_{\text{mix}}G^E_{\text{Al–Si melt}} \tag{11}$$

Here $\Delta_{\text{mix}}G^E_{\text{Al–Si melt}}$ denotes the excess Gibbs energy for mixing in the Al–Si melt [17,18], which can be expressed as the following Eq. (12)

$$\Delta_{\text{mix}}G^E_{\text{Al–Si melt}} = X_{\text{Al in Al–Si melt}}RT \ln \gamma_{\text{Al in Al–Si melt}}$$
$$+ X_{\text{Si in Al–Si melt}}RT \ln \gamma_{\text{Si in Al–Si melt}} \tag{12}$$

By substituting the $\ln X_{\text{Ti(l) in melt}}X^2_{\text{B(l) in melt}}$ in the Al–Ti–B system from Yoshikawa's work [19] listed in Table 2 into Eq. (9), the extrapolation of the activity coefficients of Ti–2B in molten Al can be expressed as Eq. (13)

$$RT \ln \gamma_{\text{Ti(l) in molten Al}}\gamma^2_{\text{B(l) in molten Al}} = -15938 + 25.75T \tag{13}$$

Taking the results of Eqs. (12) and (13) and the $\ln X_{\text{Ti(l) in melt}}X^2_{\text{B(l) in melt}}$ in the Al–Si–Ti–B system [13] into Eq. (11), the product of the activity coefficients of Ti–2B in hypothetical molten Si at 1173 K and 1273 K are determined as:

$$RT \ln \gamma_{\text{Ti(l) in molten Si}}\gamma^2_{\text{B(l) in molten Si}}$$
$$= \begin{cases} -107290.9 \ (T = 1273K) \\ -112220.3 \ (T = 1173K) \end{cases}$$

With the assumption that the excess partial molar Gibbs energy is the formula $RT \ln \gamma_i = a + bT$ (i: B or Ti), the temperature dependence of it is expressed by Eq. (14):

$$RT \ln \gamma_{\text{Ti(l) in molten Si}}\gamma^2_{\text{B(l) in molten Si}} = -170042 + 49.29T \tag{14}$$

For the $X_{\text{Si in Al–Si melt}}$ in this Al-29.3at.%Si system can be calculated as a function of the temperature from Al–Si phase diagram:

Table 2
Results for the solubilities of Ti–2B atoms group in molten Al and Al–Si melt [13,19].

System	Temperature	$\ln X_{\text{Ti(l) in melt}} X^2_{\text{B(l) in melt}}$
Al–Ti–B system [19]	1373	−27.93
	1473	−25.78
	1573	−23.73
Al-35.4 at.% Si–Ti–B system [13]	1173	−29.95
Al-40.0 at.% Si–Ti–B system [13]	1273	−26.76

$$X_{\text{Si in Al–Si melt}} = \begin{cases} -0.940 + 2.34 \times 10^{-3}T - 1.83 \times 10^{-6}T^2 + 6.54 \times 10^{-10}T^3 & (850 \leq T < 1123\text{K}) \\ 0.293 & (T \geq 1123\text{K}) \end{cases} \tag{15}$$

Then the $RT \ln \gamma_{\text{Ti(l) in Al–Si melt}} \gamma^2_{\text{B(l) in Al–Si melt}}$ at different temperatures can be calculated by combining Eqs. (11)–(15). And substituting the results of $RT \ln \gamma_{\text{Ti(l) in Al–Si melt}} \gamma^2_{\text{B(l) in Al–Si melt}}$ into Eq. (9), temperature dependence of $X_{\text{Ti(l) in Al–Si melt}} X^2_{\text{B(l) in Al–Si melt}}$ is calculated and shown in Fig. 5. The relationship between temperature and the Ti (B) contents in the Al–Si melt is clarified, which indicates that the effectiveness of B removal from the primary Si phase in the Al–Si melt requires excessive Ti addition or lower temperature.

3.4. Precipitation process of TiB₂ in Al–Si melts

Precipitation of the TiB₂ in the Al–Si melts could be calculated by the following reaction, when x mole TiB₂ precipitate, Ti(l) and B(l) in the Al–Si melts decrease x mole and $2x$ mole respectively.

$$\begin{array}{cccc} \text{Ti(l)} + & 2\text{B(l)} = & \text{TiB}_2(\text{s}) \\ x & 2x & x \end{array} \tag{16}$$

Then combining with the initial contents of Ti(B) listed in Table 1 and the temperature dependence of the $X_{\text{Ti(l) in Al–Si melt}} X^2_{\text{B(l) in Al–Si melt}}$ in Fig. 5, the formula can be written as Eq. (17)

$$(X_{\text{Ti ini}} - x)(X_{\text{B ini}} - 2x)^2 = X_{\text{Ti(l) in Al–Si melt}} X^2_{\text{B(l) in Al–Si melt}} \tag{17}$$

Then the $X_{\text{Ti(l) in Al–Si melt}}$ and $X_{\text{B(l) in Al–Si melt}}$ at different temperatures can be calculated by Eq. (17). For the $X_{\text{B(l) in Al–Si melt}}$ falls at a relatively high rate, Fig. 6 shows the $X_{\text{Ti(l) in Al–Si melt}}$ and

$X_{\text{B(l) in Al–Si melt}}$ in a temperature range between the melting temperature (1323 K) and the liquidus temperature (T_L) (1123 K), which indicates that the TiB₂ particles precipitate before the primary Si growth. In sample E-1, the B content in the Al–Si melt remains the initial content without Ti addition. In sample E-2, because the initial B content in the Al–Si melt is excessive, when the Ti content in the Al–Si melt reaches a low level, the B content in the Al–Si melt remains unchanged. In sample E-3, because the initial B and Ti contents in the Al–Si melt are nearly 2:1, during the solidification, both B and Ti contents decrease and reach a low level. In sample E-4, because the initial Ti content in the Al–Si melt is excessive, the B content in the Al–Si melt falls and reaches a low level, a relatively high B removal is achieved.

In all the above calculations about the B(Ti) contents in the Al–Si melt, only thermodynamic factors of the reaction are considered. When kinetic factors are considered, the reaction rate can be expressed by:

$$\frac{dc_{\text{TiB}_2}}{dt} = k \cdot [\text{Ti}]^m \cdot [\text{B}]^n \tag{18}$$

where m and n are the reaction order of Ti and B, k is a constant of reaction rate, [Ti] and [B] are Ti and B contents in the Al–Si melt. Because all the samples have the same cooling condition (cooling rate and thermal field) and the TiB₂ particles will precipitate before the primary Si growth, the relationship between the B content in the Al–Si melt at T_L (1123 K) and the B content in the primary Si should follow the same law. By comparing the B content in the Al–Si melt at T_L with the B content in the primary Si of sample E-1, $\overline{X^{\text{E-1}}_{\text{B in primary Si}}} \approx 0.8 \times X^{\text{E-1}}_{\text{B in Al–Si melt}}$ (1123K), B is barely removed in the Al–Si system without Ti addition. In sample E-2, when [Ti]
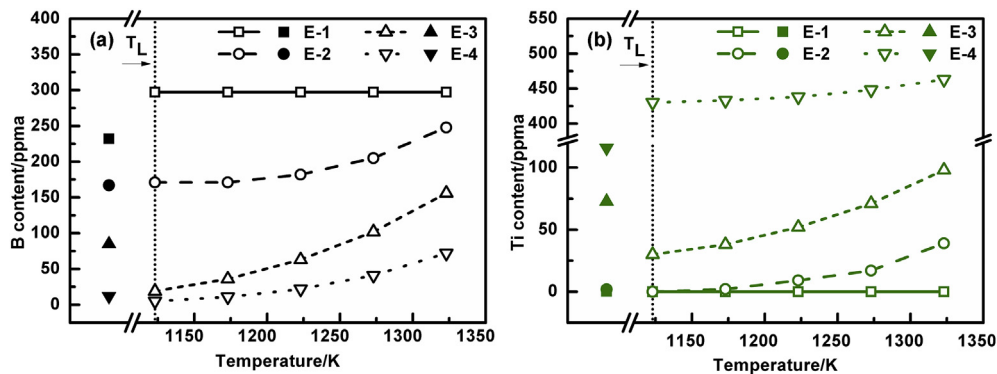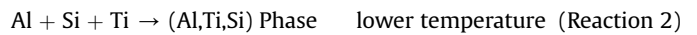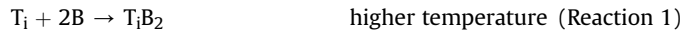

Fig. 6. Calculated B(Ti) contents in the Al–Si melt (open symbol) at different temperatures compared with average B(Ti) contents in the primary Si(solid symbol) in each sample, (a) B contents, (b) Ti contents.

reaches a low level, the reaction rate (dc_{TiB2}/dt) decreases, so $\overline{X_{B \text{ in primary Si}}^{E-2}} \approx X_{B \text{ in Al–Si melt}}^{E-2}$(1123K). In sample E-3, both [Ti] and [B] decrease and reach a low level, so $\overline{X_{B \text{ in primary Si}}^{E-3}} \gg X_{B \text{ in Al–Si melt}}^{E-3}$(1123K). In sample E-4, because the [Ti] is excessive, when [B] reaches a low level, the reaction rate (dc_{TiB2}/dt) decreases, so $\overline{X_{B \text{ in primary Si}}^{E-4}} \approx X_{B \text{ in Al–Si melt}}^{E-4}$(1123K). Because the reaction rate depends on both [Ti] and [B], when the thermodynamic factors and the kinetic factors of the reaction are considered, adding excessive [Ti] is an efficient method to removal B in the primary Si.

In order to understand the Ti distribution behavior during cooling, the microstructure of sample E-4 is observed by BSE microanalysis. Fig. 7(a) shows that the structure comprises of dark matrix Al (point A), gray distinctive needle-like eutectic Si phases (point B) and light-colored spherical intermetallic compounds (point C). Fig. 7(b) shows the EDS spectrum of the cross spot, which indicates that these spherical intermetallic compounds are TiB$_2$ particles. The detailed lattice parameters of Si and TiB$_2$ calculated by the software of CASTEP are summarized in Fig. 7(c). Because Si has quite different space group and lattice parameters from that of TiB$_2$, even the TiB$_2$ particles precipitate before the primary Si formation, the TiB$_2$ particles can't act as the nuclei of the primary Si or be trapped by the growing primary Si phase. The TiB$_2$ particles absorb the B atoms in the nearby melt continuously during the solidification and hence reduce the B content in the primary Si with more Ti addition. Because the eutectic Si formation is a non-equilibrium process at a relatively high rate as compared with that of the primary Si, the TiB$_2$ particles in Fig. 7 are cladded by the quick growing eutectic Si phases but not the primary Si phase.

From the discussion above, it is concluded that the TiB$_2$ particles precipitate before the primary Si and can't be easily trapped by the growing primary Si phase, the increasing Ti contents in the primary Si with the increasing Ti addition must be followed by another mechanism. Fig. 6 (b) shows that the average Ti contents in the primary Si in sample E-3 and E-4 are higher than that in sample E-1 and E-2. In the primary Si flakes after acid leaching, deionized water washing and drying, a large number of these flakes are half coated with a blue film, which can be easily observed by naked eye. Fig. 8(a) shows the macrostructure of a piece of these primary Si flakes half coated with a blue film (marked by red line). Fig. 8(b) shows the SEM image of the edge part of the blue film, the upper part is the blue film and the lower part is the surface of the primary Si phase. The upper part (blue film) in SEM image is a white film with many bulb-like pores, while the lower part in SEM image is a plain with many steps. Fig. 8(c) shows the EDS results of the cross spot in Fig. 8(b), indicating that the blue film contains Si, Ti and Al. Because the film might be thinner than the EDS detection depth, the atom ratios of Al, Ti and Si are not listed here. This blue film must be a (Al,Ti,Si) ternary phase, which might be a τ phase because the low formation temperature [20–22]. Therefore from these EDS results, a competitive reaction mechanism is proposed, that is, at lower temperature, Ti atoms in the Al–Si melt will combine with Al and Si atoms, form the (Al,Ti,Si) ternary phase and be trapped by the growing primary Si phase:

$$T_i + 2B \rightarrow T_iB_2 \qquad \text{higher temperature (Reaction 1)}$$

$$Al + Si + Ti \rightarrow (Al,Ti,Si) \text{ Phase} \qquad \text{lower temperature (Reaction 2)}$$

In sample E−3, when [B] and [Ti] both reach a low level, the reaction rate of (reaction 1) decreases while the rest [Ti] follows the competitive reaction mechanism and forms the (Al,Ti,Si) phase (reaction 2), which further decreases the [Ti] and makes more [B] remain in the melt, resulting in $\overline{X_{B \text{ in primary Si}}^{E-3}} \gg X_{B \text{ in Al–Si melt}}^{E-3}$(1123K). And in sample E-4, because [Ti] is excessive, after completely reacts with [B] (reaction 1), the
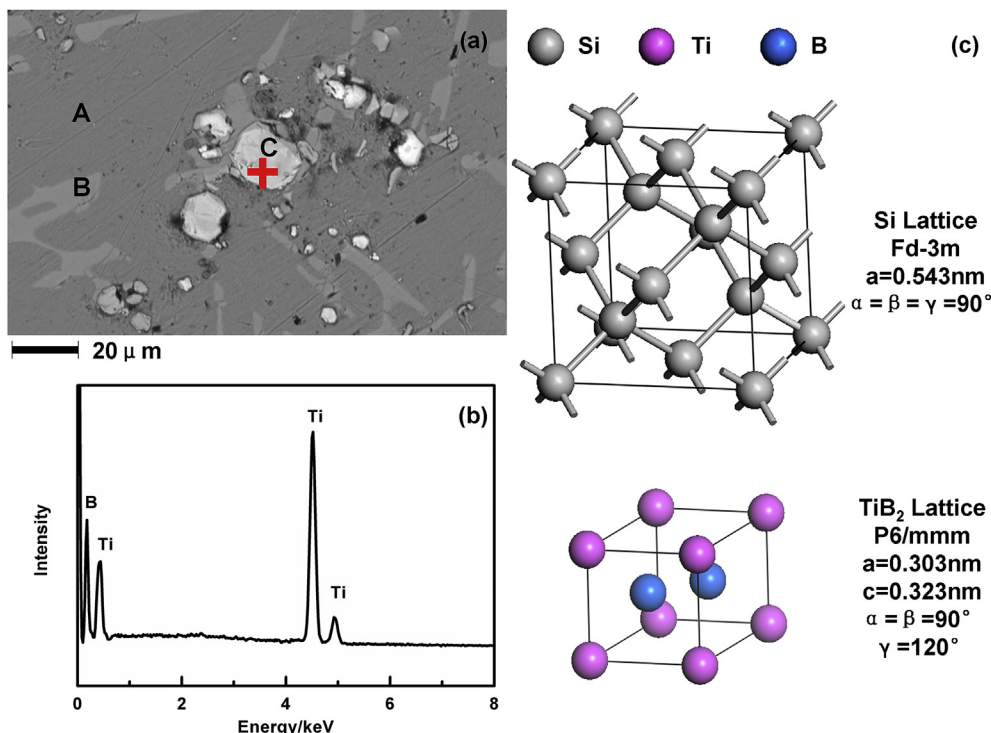

Fig. 7. (a) BSE image of TiB$_2$ particles (light-colored phase in spot C), (b) EDS spectrum of the cross spot in the BSE image, (c) lattice parameters of Si and TiB$_2$.
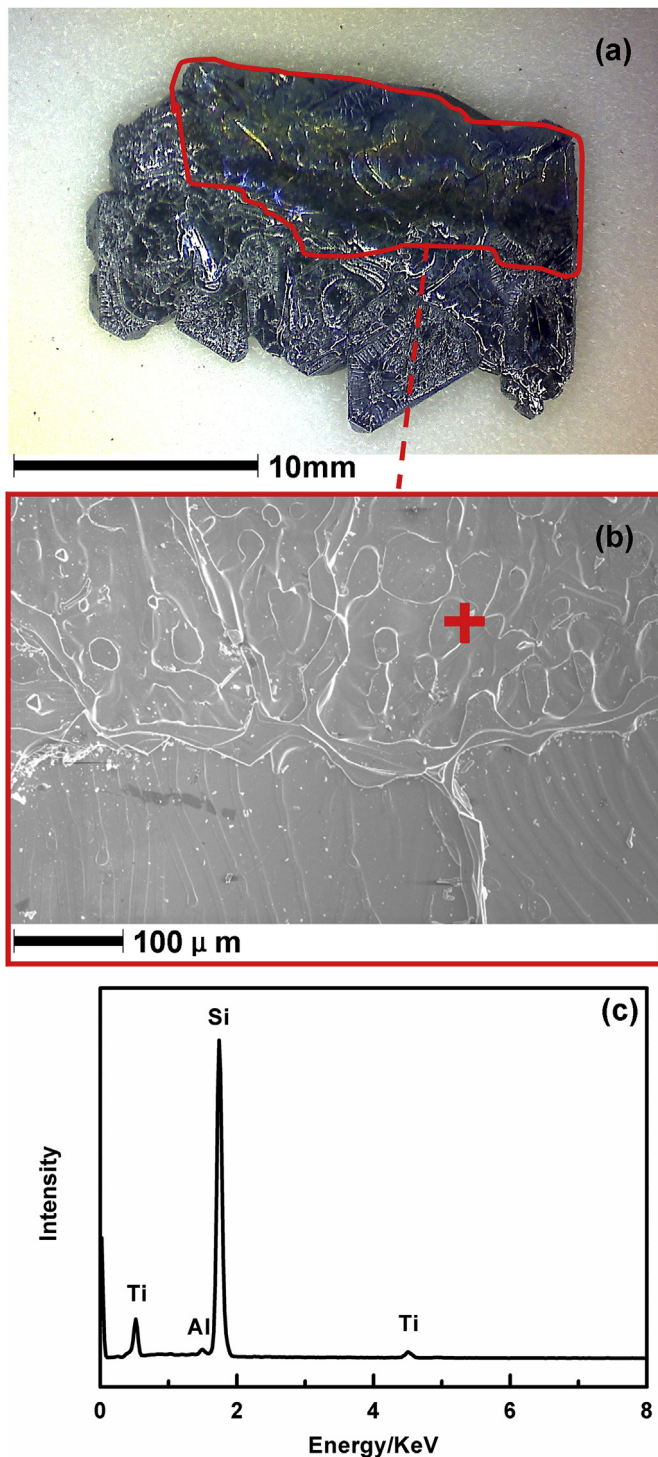
Fig. 8. (a) Macrostructure of a primary Si flake half coated with a blue film (marked by red line), (b) SEM image of the edge of the blue film, (c) EDS spectrum of the cross spot in the SEM image. (For interpretation of the references to color in this figure legend, the reader is referred to the web version of this article.)

rest [Ti] combines with Al and Si (reaction 2). So the Ti contents in the primary Si increase.

The manufacture of SoG-Si using solvent refining might be improved by the mechanism of formation of the TiB$_2$ particles discussed above. (1) From the high B removal rate in this research, the B content in the raw materials (MG-Si) is not a sensitive factor

controlling the B content of the refined Si. This finding will greatly broaden the source of the raw materials (MG-Si) used in the Si refining and reduce the cost of the SoG-Si production. (2) From the competitive reaction mechanism, excessive Ti addition should be used to make sure that the [B] reacts with [Ti] and forms TiB$_2$ priorly and completely. (3) From the formation of the (Al,Ti,Si) phase, electromagnetic stirring [23], or slow cooling [11] should be used to improve solute homogenization in the melt. These processes might avoid the (Al,Ti,Si) particles formation near the S/L interface and being trapped by the quick growing Si phase, which needs more future study.

4. Conclusions

1) High removal rates of B in the refined primary Si are achieved, resulting from the formation of the TiB$_2$ particles that reduces the B content in the Al—Si melt. The apparent segregation coefficient of B in this work is 0.0471 for Al-29.3 at% Si with 575 ppma Ti addition. In contrast, Ti addition has no effect on P removal.
2) The temperature dependence of the $X_{\text{Ti(l) in Al—Si melt}}$, $X^2_{\text{B(l) in Al—Si melt}}$, individual Ti and B contents in the Al-29.3at.%Si melt from 1323 to 1123 K are evaluated. The result indicates that the TiB$_2$ particles precipitation prior to the primary Si growth is the mechanism for the high B removal rate.
3) A new competitive reaction mechanism is proposed:

   1 $T_i + 2B \rightarrow T_iB_2$ higher temperature
   2 $Al + Si + Ti \rightarrow$ (Al,Ti,Si) Phase   lower temperature

The excessive Ti in the melt combines with Al and Si and forms (Al,Ti,Si) phase at lower temperature, resulting in an increasing Ti contents in the primary Si phase.

References

[1] S. Ranjan, S. Balaji, R.A. Panella, B.E. Ydstie, Silicon solar cell production, Comput. Chem. Eng. 35 (2011) 1439—1453.
[2] A.F.B. Braga, S.P. Moreira, P.R. Zampieri, J.M.G. Bacchin, P.R. Mei, New processes for the production of solar-grade polycrystalline silicon: a review, Sol. Energy Mater. Sol. Cells 92 (2008) 418—424.
[3] M.D. Johnston, L.T. Khajavi, M. Li, S. Sokhanvaran, M. Barati, High-Temperature Refining of Metallurgical-Grade Silicon: a Review, JOM 64 (2012) 935—945.
[4] L. Zhang, Y. Tan, J. Li, Y. Liu, D. Wang, Study of boron removal from molten silicon by slag refining under atmosphere, Mat. Sci. Simicon. Prog. 16 (2013) 1645—1649.
[5] J. Wang, X. Li, Y. He, N. Feng, X. An, F. Teng, C. Gao, C. Zhao, Z. Zhang, E. Xie, Purification of metallurgical grade silicon by a microwave-assisted plasma process, Sep. Purif. Technol. 102 (2013) 82—85.
[6] T. Yoshikawa, K. Morita, An Evolving Method for Solar-Grade Silicon Production: Solvent Refining, JOM 64 (2012) 946—951.
[7] F.A. Trumbore, Solid Solubilities of Impurity Elements in Germanium and Silicon, Bell Syst. Tech. J. 39 (1960) 205—233.
[8] N. Nakamura, H. Baba, Y. Sakaguchi, Y. Kato, Boron removal in molten silicon by a steam-added plasma melting method, Mater. Trans. 45 (2004) 858—864.
[9] T. Yoshikawa, K. Morita, Removal of B from Si by solidification refining with Si-Al melts, Metall. Mater. Trans. B 36 (2005) 731—736.
[10] T. Yoshikawa, K. Morita, Removal of phosphorus by the solidification refining with Si-Al melts, Sci. Technol, Adv. Mat. 4 (2003) 531—537.
[11] Y. Li, J. Chen, B. Ban, T. Zhang, S. Dai, Effect of Cooling Rate on Boron Removal and Solidification Behavior of Al-Si Alloy, High. Temp. Mater. Process. 34 (2015) 43—49.
[12] D. Sollmann, Pure and Simple, Phot. Int. 5 (2009) 110—113.

[13] T. Yoshikawa, K. Arimura, K. Morita, Boron Removal by Titanium Addition in Solidification Refining of Silicon with Si-Al Melt, Metall. Mater. Trans. B 36 (2005) 837—842.

[14] M.D. Johnston, M. Barati, Calcium and titanium as impurity getter metals in purification of silicon, Sep. Purif. Technol. 107 (2013) 129—134.

[15] B. Ban, X. Bai, J. Li, Y. Li, J. Chen, S. Dai, The Mechanism of P Removal by Solvent Refining in Al-Si-P System, Metall. Mater. Trans. B 46 (2015) 2430—2437.

[16] G.W. Toop, Predicting Ternary Activities Using Binary Data, Trans. TMS-AIME 233 (1965) 850—855.

[17] A. Kostov, D. Živković, B. Friedrich, Thermodynamic Predicting of Si-Me (Me = Ti, Al) Binary Systems, J. Min. Met. 43 (2007) 29—38.

[18] J.L. Murray, A.J. McAlister, The Al-Si (Aluminum-Silicon) system, Bull. Alloy Phase Diagrams 5 (1984) 74—84.

[19] T. Yoshikawa, K. Morita, Thermodynamics of Titanium and Boron in Molten Aluminum, J. Jpn. Inst. Met. 68 (2004) 390—394.

[20] O. Dezellus, B. Gardiola, J. Andrieux, M. Lomello-Tafin, J.C. Viala, On the Liquid/Solid Phase Equilibria in the Al-Rich Corner of the Al-Si-Ti Ternary System, J. Phase Equilib. Diff 35 (2014) 137—145.

[21] Z. Li, C. Liao, Y. Liu, X. Wang, Y. Wu, M. Zhao, Z. Long, F. Yin, 700°C Isothermal Section of the Al-Ti-Si Ternary Phase Diagram, J. Phase Equilib. Diff 35 (2014) 564—574.

[22] Q. Luo, Q. Li, J.Y. Zhang, S.L. Chen, K.C. Chou, Experimental investigation and thermodynamic calculation of the Al-Si-Ti system in Al-rich corner, J. Alloys Comp. 602 (2014) 58—65.

[23] B. Ban, Y. Li, Q. Zuo, T. Zhang, J. Chen, S. Dai, Refining of metallurgical grade silicon by solidification of Al-Si melt under electromagnetic stirring, J. Mater. Process. Tech. 222 (2015) 142—147.